

Thermal Decomposition of 1,5-Dinitrobiuret (DNB): Direct Dynamics Trajectory Simulations and Statistical Modeling

Jianbo Liu*

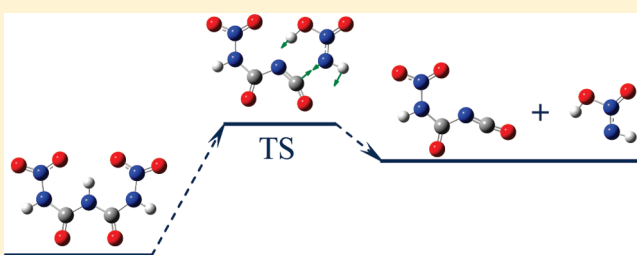
Department of Chemistry and Biochemistry, Queens College and the Graduate Center of the City University of New York, 65-30 Kissena Boulevard, Flushing, New York 11367, United States

Steven D. Chambreau[†] and Ghanshyam L. Vaghjiani[‡][†]ERC, Inc.[‡]Air Force Research Laboratory, AFRL/RZSP, Propulsion Directorate, Edwards Air Force Base, California 93524, United States

Supporting Information

ABSTRACT: A large set of quasi-classical, direct dynamics trajectory simulations were performed for decomposition of 1,5-dinitrobiuret (DNB) over a temperature range from 4000 to 6000 K, aimed at providing insight into DNB decomposition mechanisms. The trajectories revealed various decomposition paths and reproduced the products (including HNCO, N₂O, NO₂, NO, and water) observed in DNB pyrolysis experiments. Using trajectory results as a guide, structures of intermediate complexes and transition states that might be important for decomposition were determined using density functional theory calculations.

Rice–Ramsperger–Kassel–Marcus (RRKM) theory was then utilized to examine behaviors of the energized reactant and intermediates and to determine unimolecular rates for crossing various transition states. According to RRKM predictions, the dominant initial decomposition path of energized DNB corresponds to elimination of HNNO₂H via a concerted mechanism where the molecular decomposition is accompanied with intramolecular H-atom transfer from the central nitrogen to the terminal nitro oxygen. Other important paths correspond to elimination of NO₂ and H₂NNO₂. NO₂ elimination is a simple N–N bond scission process. Formation and elimination of nitramide is, however, dynamically complicated, requiring twisting a –NHNO₂ group out of the molecular plane, followed by an intramolecular reaction to form nitramide before its elimination. These two paths become significant at temperatures above 1500 K, accounting for >17% of DNB decomposition at 2000 K. This work demonstrates that quasi-classical trajectory simulations, in conjunction with electronic structure and RRKM calculations, are able to extract mechanisms, kinetics, dynamics and product branching ratios for the decomposition of complex energetic molecules and to predict how they vary with decomposition temperature.



I. INTRODUCTION

1,5-Dinitrobiuret (DNB, C₂H₃N₅O₆, molecular weight = 193.08) is a very powerful and promising new explosive.^{1–4} This nitrogen-rich compound was first synthesized by Thiele and Uhlfelder in 1898.⁵ Recently, Klapötke and co-workers reported both experimental and theoretical studies of DNB, which determined the DNB molecular structure, energetics, pyrolysis as well as detonation velocity and pressure.^{1–3} DNB has an approximate planar structure, and the standard heat of formation ($\Delta_f H$) was calculated to be –353 kJ/mol (–1829 kJ/kg) at the MP2/cc-pVTZ level of theory.² The enthalpy ($\Delta_r H$) for the reaction of DNB(s) \rightarrow 2CO₂(g) + 3/2 H₂O(l) + 1/4 O₂(g) + 5/2 N₂(g) was determined to be 1003 \pm 39 kJ/mol (5195 \pm 200 kJ/kg) using bomb calorimetry.² DNB detonated strongly in the steel sleeve test, without the need of adding any additional oxidizer. The detonation velocity and detonation pressure were calculated to be 8.66 mm/ μ s and 33.9 GPa, respectively.^{2,3} These values are

close to those of the well-established energetic materials, such as HMX⁶ (i.e., cyclotetramethylene-tetranitramine) and RDX⁶ (i.e., cyclotrimethylene-trinitramine). Thermal decomposition of DNB was examined by thermogravimetric analysis (TGA) and differential scanning calorimetry (DSC), and gaseous products were identified using mass spectrometry and Fourier transform infrared spectroscopy.^{1,4} DSC analysis revealed that thermal decomposition of DNB does not occur in a single step; instead, it has several different activated reactions. The ultimate decomposition gases include HNCO, N₂O, CO₂, and water. However, the decomposition mechanism and dynamics have not yet been clearly established. One of the challenges is that the mechanisms involving highly reactive intermediates are difficult to probe

Received: April 26, 2011

Revised: June 3, 2011

Published: June 07, 2011

experimentally, because such dissociation is a violent event and over within nanoseconds.

It is worth noting that Schneider et al. reported a hypergolic ionic liquid fuel based on dicyanamide anions with white fuming nitric acid.⁷ Hypergolic systems are fuel–oxidizer combinations that ignite spontaneously upon mixing of two propellants at low temperatures and pressures, without the presence of an external ignition source. According to the proposed mechanism for the hypergolic ignition of dicyanamide anions with nitric acid, the reaction sequence results in the formation of DNB as an intermediate in the ignition process.⁴ Therefore, a detailed understanding of the mechanisms and dynamics of DNB decomposition is necessary for constructing an accurate kinetics model to predict the fuel performance, for optimizing the design of propulsion systems using hypergolic bipropellants, and for modifying and designing new fuels.

In the present study, thermal decomposition of DNB was probed theoretically. For complex molecules, especially for those with a high internal energy content, use of chemical intuition to predict reaction pathways can prove unreliable. There may be concerted reactions that are difficult to predict, and once energy stored in the molecule begins to release, the system does not necessarily follow the minimum energy reaction path, i.e., the subsequent behavior is controlled by dynamics.⁸ Even for the steps in the reaction that are controlled by statistical factors, standard transition-state locating methods may be difficult to apply, because the molecular transformations are too complex. A useful approach to treating such a system is quasi-classical, direct dynamics trajectory simulations, where the motion of the molecule is followed, allowing the molecule to “show us” what the preferred reaction pathways are. The direct dynamics method dispenses with the potential energy surface. Instead, it calculates the energies, force constants, and Hessian “on the fly” using quantum chemistry methods.^{9–17} This method becomes computationally attractive when the dimensionality of the system increases, particularly for the DNB molecule, which contains 13 heavy atoms. Dynamics simulations partition the energy generated by exothermic reactions to vibrational, rotational, and translational modes, increasing the chance of locating new reaction pathways. In addition, by following the variation of the potential energy during the trajectory rather than relying on intuition, we can identify better geometries for TS searching, as demonstrated below.

The remainder of the paper is organized as follows. Section II describes the methods of electronic structure/statistical calculations and quasi-classical trajectory simulations used to determine the thermal decomposition features of DNB. Trajectory simulation results are presented in Section III, including an overview of the nature and time scales of trajectories we are simulating, the prescription for sorting trajectories, and contributions of various decomposition mechanisms at different temperatures. Statistical modeling results are presented in section IV, starting with construction of the reaction coordinate for DNB decomposition using density functional theory electronic structure calculations, proceeding to decomposition product branching using Rice–Ramsperger–Kassel–Marcus (RRKM) theory,¹⁸ and finally to the analysis of interconversions of primary decomposition products. Conclusions are presented in section V.

II. COMPUTATIONAL METHODOLOGY

A. Electronic Structure and RRKM Calculations. To aid in reaction coordinate interpretation and to get energetics

information, density functional theory (DFT) electronic structure calculations were performed at the B3LYP/6-31++G** level of theory, using the Gaussian 09 (B.01) suite of programs.¹⁹ Geometries were optimized by calculating force constants at every step. Vibrational frequencies and zero-point energies (ZPE) were scaled by a factor of 0.955 and 0.981,²⁰ respectively. The corrected ZPE were added to the stationary point energies. All the transition states (TSs) found were verified to be first-order saddle points by frequency calculations, and the vibrational mode with the imaginary frequency corresponds to the reaction coordinate. When necessary, intrinsic reaction coordinate (IRC) calculations were used to determine which minima are connected by a particular TS. To obtain more accurate energies of the reactant and products, calculations were also performed at the MP2/cc-pVDZ level of theory.

A transition-state-theory-based statistical model, the RRKM theory,¹⁸ was employed to examine the properties of the reactant, intermediate complex, and transition states as a function of the total internal energy and associated angular momentum. The fundamental assumption in the RRKM model is that energy is randomized and distributed statistically among all the energetically accessible states of the system, and the rate of a particular process (e.g., dissociation of a molecule or interconversion between different isomers) is proportional to the total number of energetically accessible states at the transition state.^{21,22} As a consequence, statistical reactions tend to occur by paths close to the minimum energy path, as the density of states is highest for such paths.²³ RRKM unimolecular rates for crossing various transition states and density of states were calculated with the program of Zhu and Hase,²⁴ using its direct count algorithm, and scaled frequencies and energetics from the DFT calculations. The angular momentum quantum number J used for RRKM calculations was determined from the corresponding DNB rotational energy, assuming DNB can be roughly treated as a nearly symmetric top molecule because two of the principle moments of inertia are not very different. Product branching is given by the ratio of the RRKM rates.

B. Quasi-Classical Direct Dynamics Trajectory Simulations. In this study, direct dynamics trajectory simulations were conducted for two purposes: (1) investigating decomposition mechanisms of DNB at various temperatures and discovering decomposition products²⁵ and (2) locating key transition states for important decomposition paths, when the standard TS-searching methods (i.e., TS, QST2, and QST3 methods in Gaussian) fail.^{26,27} Trajectory simulations started at the equilibrium geometry of DNB. A general chemical dynamics program VENUS of Hase et al.²⁸ was used to set up the trajectory initial conditions, and the Hessian-based method of Bakken et al.¹⁷ implemented in Gaussian was used to propagate each trajectory with Hessians recalculated every five steps. The integrations were performed with a step size of ~ 0.4 fs, which conserved the total energy to better than 10^{-4} Hartree. The SCF = XQC option was used during trajectory integration so that a quadratically convergent Hartree–Fock (QC-SCF) method^{19,29} was adopted in case that the usual, but much faster, first-order SCF method did not converge within the allotted number of cycles. Because millions of gradient and Hessian evaluations were required, the level of theory used for simulations was necessarily modest. To select a suitable level of theory, we calculated the enthalpy of combustion of DNB,² i.e., $\Delta_r H$ for $C_2H_3N_5O_6(s) \rightarrow 2CO_2(g) + 3/2H_2O(l) + 1/4O_2(g) + 5/2N_2(g)$, using B3LYP and MP2 methods with 6-31G, 6-31G*, 6-31+G*, and 6-31++G** basis sets. The enthalpy of vaporization

Table 1. Calculated Enthalpy of Detonation ($\Delta_r H$) of DNB (kJ/mol)

| | methods | | | | |
|--------------|-------------|--------------|---------------|-----------------|--------------------------|
| | B3LYP/6-31G | B3LYP/6-31G* | B3LYP/6-31+G* | B3LYP/6-31++G** | MP2/cc-pVTZ ^a |
| $\Delta_r H$ | -606 | -695 | -739 | -757 | -863 |

^a Reference 2.

Table 2. Calculated DNB Vibrational and Rotational Energies at Various Temperatures

| | T/K | | | | | | | | | | |
|----------------------------|------|------|------|------|------|------|------|------|-------|-------|-------|
| | 298 | 500 | 750 | 1000 | 1250 | 1500 | 1750 | 2000 | 4000 | 5000 | 6000 |
| E_{vib}/eV | 0.26 | 0.65 | 1.27 | 1.99 | 2.76 | 3.57 | 4.40 | 5.24 | 12.25 | 15.82 | 19.41 |
| E_{rot}/eV | 0.04 | 0.06 | 0.10 | 0.13 | 0.16 | 0.19 | 0.23 | 0.26 | 0.52 | 0.65 | 0.78 |

of water (44.00 kJ/mol) was taken from the NIST database,³⁰ and the enthalpy of sublimation of DNB was assumed to be close to that of biuret² (which is -126.7 kJ/mol from NIST³⁰). We then compared these results to the reported benchmark calculation at the electron-correlated MP2/cc-pVTZ level of theory,² and the results are listed in Table 1. It was found that the MP2 method ran into a convergence problem for DNB with the selected basis sets. Compared with MP2/cc-pVTZ, all B3LYP methods underestimate $\Delta_r H$; however, including polarization in basis sets significantly improves the accuracy of DFT energetics. (Note that none of the calculated $\Delta_r H$ values, including the MP2/cc-pVTZ value, perfectly match the experimental determined enthalpy of detonation of 1003 kJ/mol, which is most likely due to uncertainty arising from the estimated enthalpy of DNB sublimation and different structures of DNB in the gas phase and in the crystalline state.²) On the basis of the overall level of agreement and computational speed, the B3LYP/6-31G* level of theory was chosen for the main set of trajectories. It is noted that the major purpose of our trajectory simulations is to probe the gross features of DNB decomposition and to identify important decomposition paths.

The initial vibrational and rotational energies of DNB were sampled from Boltzmann distributions at specified temperatures. The quasi-classical initial vibrational states were simulated by giving each reactant atom displacement from equilibrium and momentum appropriate to the initial rovibrational state, with random phases for the different modes. The molecule has zero-point energy in all vibrational models. Because the decomposition time scale at typical detonation temperatures would be far too long for practical trajectory simulations, simulations have to be carried out at high temperature. To identify a reasonable temperature range for dynamics simulations, we first ran a series of trajectories at a low level of theory, HF/6-31G, at a temperature range of 1000–8000 K. Within a trajectory simulation period of 4 ps, no dissociative trajectories were observed at temperatures below 3000 K. At a temperature of 3000 K, only 15% of total trajectories were dissociative. On the other hand, almost every trajectory underwent decomposition within a short time (<0.4 ps) at temperatures higher than 6000 K. Therefore, three temperatures, 4000, 5000, and 6000 K, were chosen for running trajectory simulations at the B3LYP/6-31G* level of theory. For each temperature, batches of trajectories (50 trajectories each) were calculated. Trajectories were propagated for a preset length of time (~4 ps), or until the distance between the decomposition

products exceeded 9.0 Å. A total of 150 trajectories were completed at the B3LYP/6-31G* level of theory in the course of the study reported here, each taking ~380 CPU hours on an Intel Core 2 dual and Core 2 quad (3.0 GHz)-based 64 bit Linux computational cluster. Thus, the complete set of trajectories required about 6.5 years of CPU time on the cluster. The program gOpenMol was used for trajectory visualization.³¹ Detailed analysis of individual trajectories and statistical analysis of the trajectory ensemble was done with programs specifically written for this purpose,^{27,32–37} available from the corresponding author upon request.

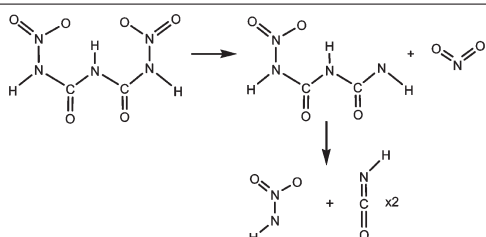
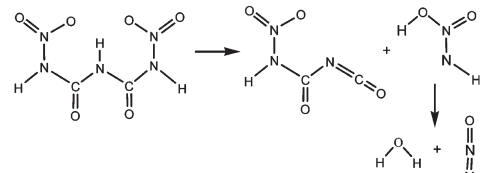
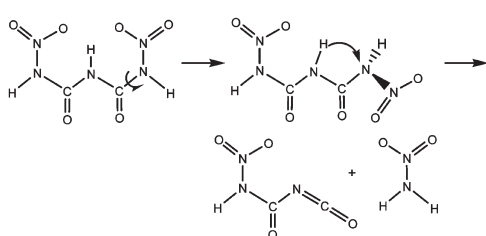
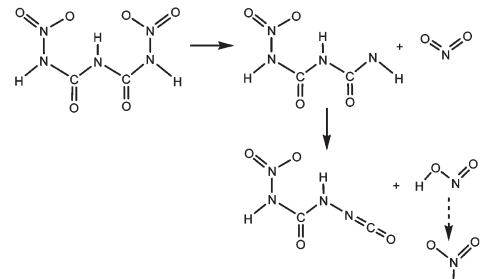
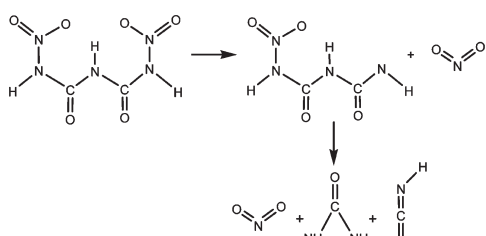
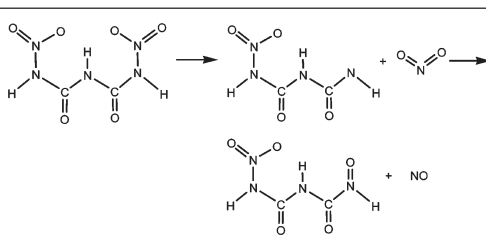
One issue with using quasi-classical trajectory methods is that vibrational energy is not quantized in molecules. Lack of quantization presumably has an effect on how energy is distributed between vibrational modes during trajectories and upon dissociation.^{38,39} It is possible to have trajectories where the product vibrational energy is below the zero-point level. Such unphysical trajectories were found to be negligible in our trajectories, presumably because we are looking at relatively high internal energies (see Table 2), reducing the errors associated with treating the motion classically.

As mentioned above, temperatures used for simulations are much higher than the detonation temperature, which was ~1500 K estimated from the temperature of the Bunsen burners used in experiments⁴⁰ (for reference, the experimentally measured DNB decomposition temperature is around 405 K).¹ Table 2 lists the estimated vibrational and rotational energies at various temperatures. As a result, some trajectories may find decomposition paths with barriers too high to be relevant to decomposition at realistic temperatures. The trajectory observables of greatest interest for our purpose are decomposition mechanisms. The point is that, with enough trajectories, *all* important reaction paths will be found, including those that control decomposition under the conditions of interest. Once decomposition paths are identified, the corresponding reaction energetics, including activation barriers, can be calculated, and only those which are able to contribute need be included in decomposition kinetics modeling.

III. TRAJECTORY RESULTS

Before we discuss the quasi-classical trajectory simulation results, it is useful to review the nature and time scales of the trajectories we are simulating. Trajectories were run at the temperature range of 4000–6000 K. At the temperature of 4000 K,

Table 3. Direct Dynamics Trajectory Simulation Results of DNB Decomposition^{a,b}

| Path | Decomposition products | ΔH^a /eV | Trajectory ratios (%) ^b | | |
|------|--|----------------------|------------------------------------|--------|--------|
| | | | 4000K | 5000K | 6000K |
| 1* |  <p>* some trajectories dissociate to NO₂, HN₂O₂ and HNCO simultaneously</p> | 1.73 2.43 | 34 ± 6 | 39 ± 7 | 43 ± 7 |
| 2 |  | 0.99 -0.93 | 26 ± 6 | 13 ± 5 | 7 ± 3 |
| 3 |  | 0.26 0.54 | 10 ± 4 | 6 ± 3 | 4 ± 2 |
| 4 |  | 1.73 0.80 1.11 | 4 ± 2 | 8 ± 4 | 10 ± 4 |
| 5 |  | 1.73 3.02 | 8 ± 4 | 13 ± 5 | 26 ± 6 |
| 6 |  | 1.73 0.92 | 0 | 5 ± 3 | 0 |
| | Sum of other dissociation paths | - | 8 ± 4 | 16 ± 5 | 10 ± 4 |
| | Non-reactive | - | 10 ± 4 | 0 | 0 |

^a Values of ΔH were calculated relative to DNB, at the B3LYP/6-31++G** level of theory. ^b Trajectory ratios were calculated based on 50 trajectories at each temperature.

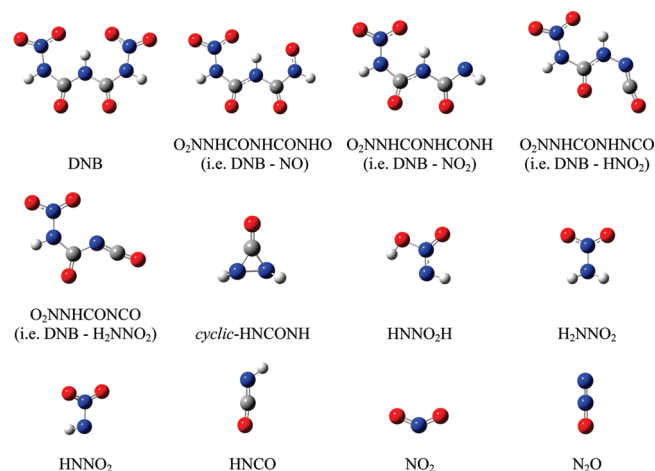


Figure 1. B3LYP/6-31++G** optimized structures of DNB and its decomposition products identified in trajectories.

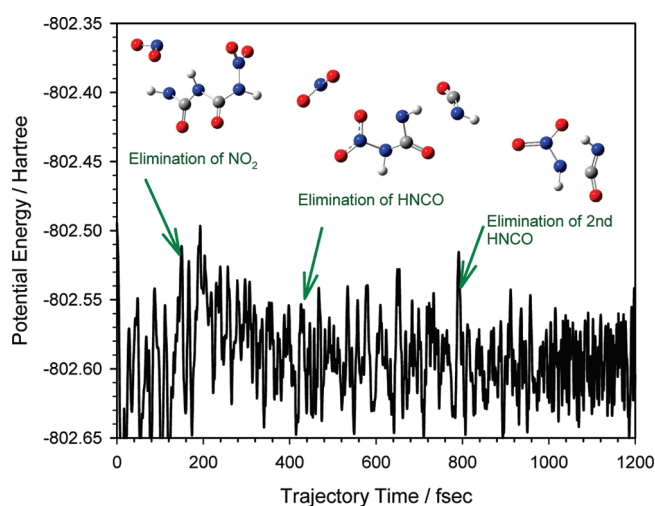


Figure 2. Representative trajectory of decomposition path 1, simulated at 4000 K using the B3LYP/6-31G* method. The plot shows variation of potential energy during the trajectory, and the snapshots show three sequential elimination steps.

10% of trajectories maintained the intact molecular structure when trajectories were terminated at 4 ps. The remaining 90% of trajectories at 4000 K and all trajectories at 5000 and 6000 K underwent thermal decomposition via direct, concerted, or sequential mechanisms before the termination of trajectories. For most of the decomposition trajectories, the time at which the DNB molecule begins decomposition is between 0.2 and 3 ps, longer than the periods of most DNB vibrational modes. The decomposition trajectories can be grouped into six classes, as summarized in Table 3. Table 3 also compares their product energetics and relative contributions (i.e., trajectory ratios) at different temperatures. The error limits given for the trajectory ratios are statistical, based on the number of total trajectories and reactive trajectories for each path, and obviously do not include any systematic errors. The structures of DNB and all decomposition products observed in trajectories are depicted in Figure 1. All these structures were optimized at the B3LYP/6-31++G** level of theory. Video files showing representative trajectories for each of the six classes are provided in the Supporting Information.

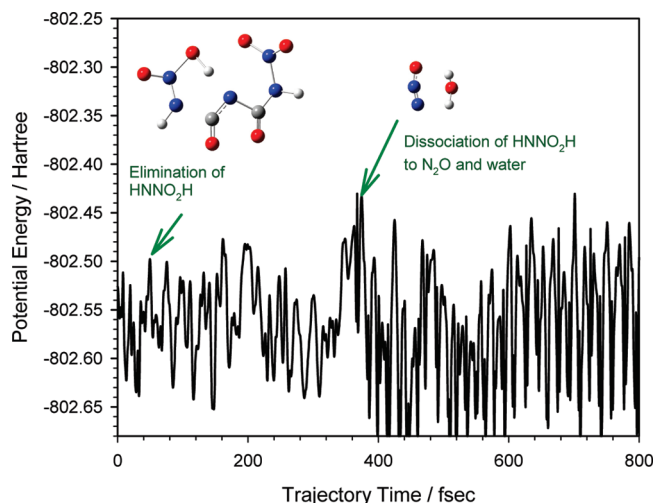


Figure 3. Representative trajectory of decomposition path 2, simulated at 4000 K using the B3LYP/6-31G* method. The plot shows variation of potential energy during the trajectory, and the snapshots show elimination of HNNO₂H and its subsequent dissociation to N₂O and water.

A. Decomposition Path 1 (Production of Isocyanic Acid and NO₂). By far, the most common outcome of DNB trajectories is path 1, which accounts for 34–43% of all trajectories at 4000–6000 K. Path 1 starts with elimination of NO₂ from DNB, followed by consecutive elimination of two isocyanic acid (HNCO) molecules from the derivative intermediate. The endothermicity of NO₂ elimination is 1.73 eV, and that of subsequent elimination of two HNCO molecules is 2.43 eV, both of which were calculated with respect to the DNB molecule. Figure 2 demonstrates a trajectory (calculated at 4000 K) representative of path 1. The figure shows the change of potential energy (PE) during the trajectory. The oscillations in the PE reflect the vibration of the DNB molecule and the products, including ZPE. The time scale of decomposition depends on the simulation temperature, but three numbers are relevant. The time between trajectory starts and the onset of NO₂ elimination is around 150 fs. The time for elimination of the first HNCO molecule from the remaining structure is around 410 fs, and the time for elimination of the second HNCO is around 800 fs. In addition to the multistep elimination process indicated in Figure 2, a small fraction of path 1 trajectories (<10%) experienced simultaneous elimination of NO₂ and HNCO.

B. Decomposition Path 2 (Production of HNNO₂H). Another common class of decomposition trajectories belongs to path 2, accounting for 7–26% of all trajectories at 4000–6000 K. In path 2, HNNO₂H is produced via intramolecular hydrogen atom transfer, followed by breaking an amide bond. HNNO₂H may further decompose to N₂O and water. While the first step is endothermic by 0.99 eV, the overall decomposition process (i.e., DNB → O₂NNHCONCO + N₂O + water) is exothermic by 0.93 eV with respect to DNB. A trajectory representative of path 2 is illustrated in Figure 3, indicating the energy barriers associated with two activated decomposition steps of which the second one is much more significant. Note that, in principle, another pathway may produce the same products as path 2, i.e., DNB completely decomposes to O₂NNHCONHCO and HNNO₂, which subsequently undergoes intermolecular hydrogen atom transfer between two fragments to produce HNNO₂H. However, this decomposition route involves breaking a CN bond with

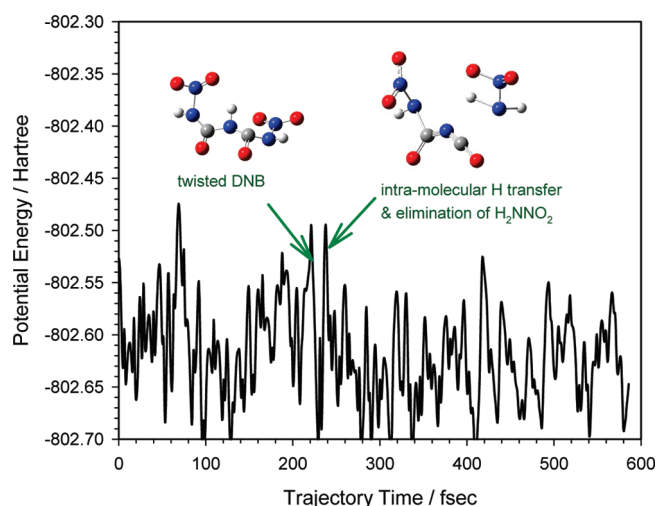


Figure 4. Representative trajectory of decomposition path 3, simulated at 4000 K using the B3LYP/6-31G* method. The plot shows variation of potential energy during the trajectory, and the snapshots show elimination of H_2NNO_2 via twisting the molecular plane, followed by intramolecular H-atom transfer.

an energy barrier in excess of 3.55 eV calculated at B3LYP/6-31++G**. Therefore, this decomposition path is less likely to contribute to a significant extent in a typical detonation.

C. Decomposition Path 3 (Production of Nitramide). Path 3 contributes to 10% of all trajectories at 4000 K, and the contribution decreases at high temperatures (6% at 5000 K and 4% at 6000 K). Figure 4 shows a typical trajectory for path 3. In this decomposition path, DNB rotates a $-\text{NHNO}_2$ unit out of the molecular plane and then undergoes an intramolecular $\text{S}_{\text{N}}\text{i}$ -reaction to form nitramide H_2NNO_2 by transferring a hydrogen atom from the central N atom to the neighboring amine N, followed by elimination of nitramide. This decomposition path has been proposed in the literature,^{1,4} and the product nitramide was identified in the mass spectrum of DNB pyrolysis products.¹ Similar to HNNO_2H , nitramide may also decompose to N_2O and water in the gas phase.¹

D. Other Decomposition Paths. The remaining trajectories can be characterized as paths 4, 5, or 6. These paths are much less common, but they are similar in that all involve sequential decomposition reactions and the first step is NO_2 elimination. In path 4, an intermolecular hydrogen atom transfer reaction occurs between two fragment compounds, $\text{O}_2\text{NNHCONHCONH}$ and NO_2 , producing $\text{O}_2\text{NNHCONHNCO}$ and nitrous acid HONO . As visualized in path 4 trajectories, when the radical fragments $\text{O}_2\text{NNHCONHCONH}$ and NO_2 (produced from a barrierless dissociation path, vide infra) separate by $\sim 3 \text{ \AA}$, roaming reorientation becomes feasible, and this leads to intermolecular H abstraction by NO_2 from $\text{O}_2\text{NNHCONHCONH}$, giving molecular product NO_2H with large vibrational excitation of the nascent O–H bond. This decomposition path is, to some extent, similar to a roaming radical reaction discovered recently.⁴¹ In some path 4 trajectories, nitrous acid interconverts to HNO_2 . At all temperatures, only 10% (or less) of all trajectories lead to path 4. In path 5, $\text{O}_2\text{NNHCONHCONH}$ undergoes extensive dissociation to NO_2 , isocyanic acid, and a three-membered ring intermediate, cyclic-HNCONH. The trajectory ratio of path 5 increases significantly at high simulation temperatures, i.e., 8% at 4000 K and increasing to 13% at 5000 K and 27% at 6000 K,

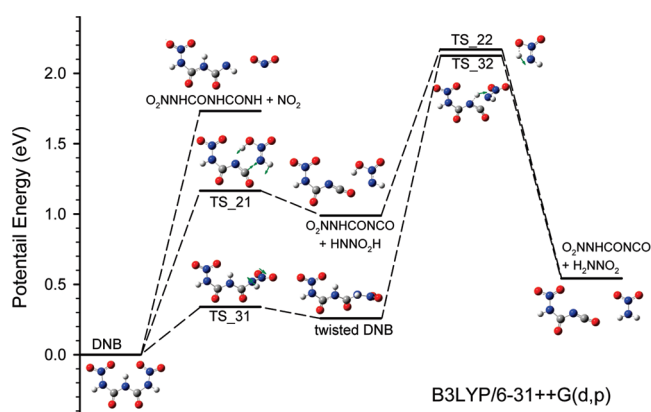


Figure 5. Schematic reaction coordinate for the initial decomposition of DNB. Energetics of complexes, TSs, and products are derived from B3LYP/6-31++G** calculations, including ZPE. For TSs, vibrational modes corresponding to the imaginary frequencies are indicated by displacement vectors.

presumably because this is the most endothermic reaction route. Finally, oxygen atom transfer between $\text{O}_2\text{NNHCONHCONH}$ and NO_2 was observed in path 6, leading to net “NO elimination” from DNB. However, path 6 only occurs at 5000 K with a ratio of 5% and was not observed at 4000 and 6000 K.

These trajectory results lead us to predict that paths 1, 2, and 3 may represent typical decomposition pathways of DNB, particularly in view of the initial decomposition steps. These paths are chosen for several considerations. First, paths 1, 2, and 3 are energetically more favorable and overall attained much higher probabilities than others in trajectory simulations. Second, the products identified in trajectories of paths 1–3, including HNCO , N_2O , NO_2 , and water, were all observed experimentally.^{1,4} Therefore, these trajectories are in reasonable agreement with experiments and can be used as a guide to extract additional mechanistic insight with confidence. On the other hand, NO (one of path 6 products) accounted for only a small amount of pyrolysis products, and HNO_2 (one of path 4 products) was not observed in pyrolysis.¹ Therefore, contributions of paths 4 and 6 are expected to be negligible. Path 5, regardless of any possible energy barriers, has an endothermicity of 3.02 eV and is, therefore, of less importance as well.

The following electronic structure calculations and statistical analysis focus on the initial decomposition steps of DNB, i.e., elimination of NO_2 , HNNO_2 , and H_2NNO_2 . It is worth noting that paths 4, 5, and 6 are all related to path 1 in that these paths share a common rate-limiting step, i.e., NO_2 elimination. Consequently, all possible decomposition paths identified in trajectory simulations are included in the present statistical modeling.

IV. RRKM MODELING

A. Reaction Coordinate. DFT calculation results for the reaction coordinate of the initial decomposition paths are summarized in Figure 5 with the DNB molecule shown at zero energy. All energetics are calculated at the B3LYP/6-31++G** level of theory. The details of the geometries for the reactant, intermediate complex, TSs, and products are available by request to the corresponding author. Structures of various TSs were optimized using a number of likely high potential energy geometries in reactive trajectories as starting geometries. NO_2 elimination

Table 4. RRKM Results for Initial Decomposition of DNB

| | temp/K | | | | | |
|------------------------|--|-------------------------|---|---|---|---|
| | 750 | 1000 | 1250 | 1500 | 1750 | 2000 |
| | density of states (1/cm ⁻¹) | | | | | |
| DNB | 1.95 × 10 ¹⁸ | 2.34 × 10 ²² | 5.98 × 10 ²⁵ | 4.94 × 10 ²⁸ | 1.71 × 10 ³¹ | 2.92 × 10 ³³ |
| twisted DNB | 1.90 × 10 ¹⁸ | 2.33 × 10 ²² | 6.04 × 10 ²⁵ | 5.04 × 10 ²⁸ | 1.75 × 10 ³¹ | 3.02 × 10 ³³ |
| | unimolecular rates (s ⁻¹) ^a | | | | | |
| <i>k</i> ₁ | 0 (0) | 0.6 (3.6) | 1.8 × 10 ⁴ (1.8 × 10 ⁵) | 2.1 × 10 ⁶ (2.7 × 10 ⁷) | 3.9 × 10 ⁷ (5.8 × 10 ⁸) | 2.9 × 10 ⁸ (4.7 × 10 ⁹) |
| <i>k</i> ₂ | 8.5 | 9.7 × 10 ⁵ | 7.9 × 10 ⁷ | 1.0 × 10 ⁹ | 5.5 × 10 ⁹ | 1.8 × 10 ¹⁰ |
| <i>k</i> ₃₁ | 3.4 × 10 ⁹ | 1.5 × 10 ¹⁰ | 3.5 × 10 ¹⁰ | 6.0 × 10 ¹⁰ | 8.8 × 10 ¹⁰ | 1.2 × 10 ¹¹ |
| <i>k</i> ₃₁ | 2.4 × 10 ¹¹ | 3.2 × 10 ¹¹ | 3.8 × 10 ¹¹ | 4.4 × 10 ¹¹ | 4.8 × 10 ¹¹ | 5.1 × 10 ¹¹ |
| <i>k</i> ₃₂ | 0 | 1.5 × 10 ⁻² | 2.1 × 10 ⁴ | 7.9 × 10 ⁶ | 2.9 × 10 ⁸ | 3.4 × 10 ⁹ |
| | branching ratios (%) ^a | | | | | |
| path 1 | 0 | 0 | 0 (0.3) | 0.2 (2.6) | 0.7 (9.1) | 1.3 (18.0) |
| path 2 | 100 | 100 | 100 (99.7) | 99.0 (96.7) | 94.3 (86.3) | 83.3 (69.2) |
| path 3 | 0 | 0 | 0 | 0.8 (0.8) | 5.0 (4.5) | 15.4 (12.8) |

^a *k*₁, *k*₂, and *k*₃₁ are the rate constants crossing TS_1, TS_21, and TS_31 from DNB, and *k*₃₁ and *k*₃₂ are the rate constants for crossing TS_31 and TS_32 from twisted DNB, respectively. The *k*₁ values in parentheses were obtained using a “loose” TS_1.

in path 1 is dynamically simple, in that no complicated rearrangement is needed for N–N bond scission. Efforts were made to locate the transition state connecting DNB to products O₂NNHCONHCONH + NO₂. However, various starting geometries corresponding to a dissociating N–N bond converged, instead, to the DNB structure at B3LYP/6-31++G** and MP2/cc-pVDZ levels of theory. We also performed a relaxed potential energy scan running along the dissociating N–N bond using the MP2/cc-pVDZ method. The N–N bond length (*r*_{NN}) was continuously varied from 1.4 to 3.1 Å, and all coordinates other than *r*_{NN} were optimized at each point. The asymptotic energy of the resulting PES scan is nearly equal to the product energy of O₂NNHCONHCONH + NO₂, suggesting that there is no substantial reverse barrier associated with decomposition to O₂NNHCONHCONH + NO₂. It is, therefore, expected that NO₂ elimination opens at the thermodynamic threshold energy of 1.73 eV and is facile. Note that previous ab initio calculations using G2 and QCISD(T)//MP2/6-311G** methods indicate that H₂N–NO₂ may dissociate to NH₂ and NO₂ without a reverse barrier,^{42,43} and our calculations are consistent with that finding.

The only low-energy route for path 2 located computationally appears to be DNB → TS_21 → O₂NNHCONCO + HNNO₂H. The reaction is endothermic by 0.99 eV; however, the decomposition path bears an energy barrier of 1.16 eV with respect to DNB. Path 3 is slightly more convoluted: DNB → TS_31 → twisted DNB → TS_32 → O₂NNHCONCO + H₂NNO₂, that is, twisting the nearly planar DNB molecule via an activation barrier, TS_31 (0.34 eV above DNB), followed by intramolecular H-atom transfer and elimination of H₂NNO₂ via the second activation barrier, TS_32 (2.13 eV above DNB). One issue for interpretation of paths 2 and 3 products is that HNNO₂H might isomerize to H₂NNO₂, which could affect the subsequent decomposition products. The TS_22 for this isomerization is 1.18 eV above the HNNO₂H energy. It is certainly possible that

interconversion might occur during the decomposition at the detonation temperature. No other low-energy pathways were found leading to decomposition paths 1, 2, and 3, although we cannot exclude the possibility that such pathways exist.

B. RRKM Results. To evaluate whether the initial decomposition paths identified in trajectory simulations can account for realistic situations, the RRKM program was used to calculate the rates for each individual path at different temperatures. To calculate the RRKM unimolecular rates, sets of vibrational frequencies and rotational constants appropriate for the reactant and the transition states leading to dissociation are required. These are derived from the frequencies and rotational constants calculated at B3LYP/6-31++G**, with the frequencies scaled by a factor of 0.955, as suggested by recent work.²⁰ The rotation quantum number *K* was treated as active in evaluating the rates *k*(*E*, *J*) so that all (2*J* + 1) *K*-levels are counted,⁴⁴ i.e.

$$k(E, J) = \frac{d}{h} \frac{\sum_{K=-J}^J G[E - E_0 - E_r^\dagger(J, K)]}{\sum_{K=-J}^J N[E - E_r(J, K)]}$$

where *d* is the reaction path degeneracy, *G* is the transition state sum of states, *N* is the reactant density of states, *E* is the system energy, *E*₀ is the unimolecular dissociation threshold, and *E*_r and *E*_r[†] are the rotational energies for the reactant and the transition state, respectively.

Because no reverse activation barrier is located for decomposition of DNB to O₂NNHCONHCONH + NO₂, vibrational frequencies appropriate to the transition state for NO₂ elimination, hereafter termed TS_1, have to be assumed for the RRKM calculation of path 1 decomposition rates. Two limiting sets of vibrational frequencies have been chosen for TS_1.^{45–49} At one

extreme, the vibrational frequencies of TS_1 are equal to those of DNB with removal of only one mode that corresponds to the reaction coordinate (i.e., the stretching mode of the dissociating N–N bond). As long as there is no reverse activation barrier for decomposition of DNB to $O_2NNHCONHCONH$ and NO_2 , this choice reflects the “tightest” TS that is possible and would provide lower limits to the unimolecular rates for path 1. At the other extreme, a TS estimate was made that consists of 33 frequencies of $O_2NNHCONHCONH$, 3 frequencies of NO_2 , and 5 transitional frequencies. The frequencies of the six transitional modes lost upon dissociation are chosen from DNB. One N–N stretching frequency is chosen as the reaction coordinate and removed. The five remaining transitional frequencies (corresponding to rotations, bends, and torsions), which become rotations and translations of completely dissociated products, are scaled by a factor of 0.5 to reflect the looseness of the transition state that changes the entropy of activation (i.e., the difference in entropy between the reactant and the TS). The choice of our scaling factor is empirical and was based on others' work. A similar scaling factor was used by Armentrout's group to assign the transitional modes in the dissociation of the energized metal ion–ligand complex, ML_x .^{45–47} Dissociations of these ML_x complexes have no reverse activation barriers, and the ion-induced dipole and ion-dipole forces result in long-range metal–ligand interactions. Therefore, the corresponding TSs must be truly “loose” TSs. The fact that the similarly scaled translational frequencies were successfully used to extract dissociation energies of ML_x by Armentrout et al.^{45–47} suggests that this scaling factor yields appropriate “loose” TSs corresponding to weak associations of the products. In the present work, we employed “tight” and “loose” TS_1, respectively, in two sets of RRKM calculations for path 1 NO_2 elimination. The tightness of the transition state significantly affects the reaction rate and thus the branching ratio, and the resulting two sets of RRKM rates provide an estimate of the range of path 1 decomposition rates.

Table 4 summarizes the RRKM results, including the densities of states (DOS) for the equilibrium and twisted DNB structures, unimolecular rates, and decomposition branching ratios. At each temperature, we used the average internal energy of the system (obtained using the rotational and vibrational partition functions of DNB; see Table 2) for calculating the density of states and rate constants. In the table, k_1 , k_2 , and k_{31} represent the rates for crossing TS_1, TS_21, and TS_31 leading from the equilibrium DNB structure, whereas k_{31} and k_{32} are the rates for crossing TS_31 and TS_32 from the twisted DNB structure, respectively. The table lists two values for k_1 at each temperature (one in parentheses), which were obtained using “tight” and “loose” TS_1, respectively. According to the values of k_{31} and k_{31} , the interconversion between equilibrium and twisted structures of DNB occurs on a time scale of ps, which is significantly shorter compared with the decomposition time scale. Therefore, the relative ratio of equilibrium and twisted DNB structures could be estimated using DOS in these structures.⁵⁰ As indicated in Table 4, the values of DOS are temperature-dependent. Because the energy of the twisted structure increases by only 0.26 eV compared to the equilibrium one, the DOS ratios for equilibrium/twisted structure are nearly 1:1 from 750 to 2000 K. Consequently, at this temperature range, DNB is best considered to be a mix of two different structures, and the average lifetime of DNB is around 10^{-6} s at 1000 K, decreasing to 10^{-9} s at 1500 K. Under this circumstance, the branching for DNB decomposition can be estimated by the ratio of k_1 , k_2 , and k_{32} .

RRKM calculations predict that, at temperatures below 1500 K, path 1 (NO_2 elimination) and path 3 (nitramide elimination) are negligible due to the high and/or tight transition states, and only path 2 (elimination of $HNNO_2H$) would be expected. Paths 1 and 3 begin to emerge at 1500 K (i.e., the typical detonation temperature⁴⁰) and become significant at high temperature. Depending on the nature of the transition state adopted for the calculations, path 1 may account for 1–9% of the initial decomposition at 1750 K and 2–18% at 2000 K. For the reason discussed above, this branching includes contributions from paths 4, 5, and 6 in addition to path 1. The branching ratio of path 3 is estimated to be 1% at 1500 K, increasing to 5% at 1750 K and 12–15% at 2000 K. Because TS_32 (for the formation of nitramide from twisted DNB) and TS_22 (for the formation of nitramide from isomerization of $HNNO_2H$) have a similar barrier height, it is anticipated that H_2NNO_2 may be produced via both routes above 1500 K.

V. CONCLUSIONS

Quasi-classical, direct dynamics trajectories for thermal decomposition of DNB were analyzed to probe the decomposition mechanisms and dynamics. The trajectories, calculated at the B3LYP/6-31G* level of theory, are able to reproduce the DNB decomposition products observed in pyrolysis experiments and reveal various decomposition paths leading to these products. RRKM theory was used to verify the significance of these decomposition paths and calculate the branching ratios at real detonation temperatures, based on the reaction coordinate constructed using trajectory results. According to RRKM analysis, elimination of $HNNO_2H$, H_2NNO_2 and NO_2 can be important at typical detonation temperatures. Although $HNNO_2H$ elimination clearly dominates at the temperature range of 750–2000 K, the contributions of the other two paths increase substantially with increasing temperature. At 2000 K, elimination of nitramide can account for more than 12% of DNB decomposition. Contribution of NO_2 elimination depends on the “tightness” of the associated transition state and would account for up to 18% of DNB decomposition should the reaction occur via a “loose” transition state. By combining direct dynamics simulations and statistical modeling, we are able to ascertain the nature of the reaction mechanisms involved in the initial decomposition of DNB. This work demonstrates the utility of direct dynamics trajectory simulations as a powerful guide for investigating decomposition mechanisms and dynamics of complex energetic molecules, locating transition states for many-atom systems, and constructing the appropriate kinetic models; subsequently, it is necessary to use RRKM or other statistical theories to get meaningful results as far as for the branching ratios at experimental temperatures are concerned.

■ ASSOCIATED CONTENT

Supporting Information. Videos (MPG files) showing representative trajectories. This material is available free of charge via the Internet at <http://pubs.acs.org>.

■ AUTHOR INFORMATION

Corresponding Author

*E-mail: jianbo.liu@qc.cuny.edu.

■ ACKNOWLEDGMENT

J.L. gratefully acknowledges the financial support received from the Air Force Research Laboratory (CUNY Research Foundation Contract No. 16348 with contractor ERC, Inc., Edwards Air Force Base) via AFOSR Contract No. FA9300-06-C-0023. The authors would like to thank Scott Anderson (University of Utah) for providing part of the computational time and for many stimulating discussions and Bill Hase (Texas Tech) for providing the VENUS program.

■ REFERENCES

- (1) Geith, J.; Holl, G.; Klapötke, T. M.; Weigand, J. J. *Combust. Flame* **2004**, *139*, 358.
- (2) Geith, J.; Klapötke, T. M.; Weigand, J.; Holl, G. *Propellants, Explos., Pyrotech.* **2004**, *29*, 3.
- (3) Klapötke, T. M. *Struct. Bonding (Berlin, Ger.)* **2007**, *125*, 85.
- (4) Chambreau, S. D.; Schneider, S.; Rosander, M.; Hawkins, T.; Gallegos, C. J.; Pastewait, M. F.; Vaghjiani, G. L. *J. Phys. Chem. A* **2008**, *112*, 7816.
- (5) Thiele, J.; Uhlfelder, E. *Justus Liebig's Ann. Chem.* **1898**, *303*, 93.
- (6) Köhler, J.; Meyer, R. *Explosivstoffe*, 9th ed.; VCH: Weinheim, 1998.
- (7) Schneider, S.; Hawkins, T.; Rosander, M.; Vaghjiani, G.; Chambreau, S.; Drake, G. *Energy Fuels* **2008**, *22*, 2871.
- (8) Liu, J.; Anderson, S. L. *Int. J. Mass Spectrom.* **2005**, *241*, 173.
- (9) Wang, I. S. Y.; Karplus, M. *J. Am. Chem. Soc.* **1973**, *95*, 8160.
- (10) Leforestier, C. *J. Chem. Phys.* **1978**, *68*, 4406.
- (11) Car, R.; Parrinello, M. *Phys. Rev. Lett.* **1985**, *55*, 2471.
- (12) Baldridge, K. K.; Gordon, M. S.; Steckler, R.; Truhlar, D. G. *J. Phys. Chem.* **1989**, *93*, 5107.
- (13) Helgaker, T.; Uggerud, E.; Jensen, H. J. A. *Chem. Phys. Lett.* **1990**, *173*, 145.
- (14) Bolton, K.; Hase, W. L.; Peslherbe, G. H. *Modern Methods for Multidimensional Dynamics Computations in Chemistry*; Thompson, D. L., Ed.; World Scientific: Singapore, 1998; p 143.
- (15) Hase, W. L., Ed. *Advances in Classical Trajectory Methods: Intramolecular and Nonlinear Dynamics*; JAI: Greenwich, CT, 1998; Vol. 1.
- (16) Sun, L.; Song, K.; Hase, W. L. *Science* **2002**, *296*, 875.
- (17) Bakken, V.; Millam, J. M.; Schlegel, H. B. *J. Chem. Phys.* **1999**, *111*, 8773.
- (18) Marcus, R. A. *J. Chem. Phys.* **1952**, *20*, 359.
- (19) Frisch, M. J.; Trucks, G. W.; Schlegel, H. B.; Scuseria, G. E.; Robb, M. A.; Cheeseman, J. R.; Scalmani, G.; Barone, V.; Mennucci, B.; Petersson, G. A.; Nakatsuji, H.; Caricato, M.; Li, X.; Hratchian, H. P.; Izmaylov, A. F.; Bloino, J.; Zheng, G.; Sonnenberg, J. L.; Hada, M.; Ehara, M.; Toyota, K.; Fukuda, R.; Hasegawa, J.; Ishida, M.; Nakajima, T.; Honda, Y.; Kitao, O.; Nakai, H.; Vreven, T.; Montgomery, J. A.; Peralta, J. E.; Ogliaro, F.; Bearpark, M.; Heyd, J. J.; Brothers, E.; Kudin, K. N.; Staroverov, V. N.; Keith, T.; Kobayashi, R.; Normand, J.; Raghavachari, K.; Rendell, A.; Burant, J. C.; Iyengar, S. S.; Tomasi, J.; Cossi, M.; Rega, N.; Millam, J. M.; Klene, M.; Knox, J. E.; Cross, J. B.; Bakken, V.; Adamo, C.; Jaramillo, J.; Gomperts, R.; Stratmann, R. E.; Yazyev, O.; Austin, A. J.; Cammi, R.; Pomelli, C.; Ochterski, J. W.; Martin, R. L.; Morokuma, K.; Zakrzewski, V. G.; Voth, G. A.; Salvador, P.; Dannenberg, J. J.; Dapprich, S.; Daniels, A. D.; Farkas, O.; Foresman, J. B.; Ortiz, J. V.; Cioslowski, J.; Fox, D. J. *Gaussian 09*, revision B. 01; Gaussian, Inc.: Wallingford, CT, 2009.
- (20) Zheng, J.; Alecu, I. M.; Lynch, B. J.; Zhao, Y.; Truhlar, D. G. *Database of Frequency Scale Factors for Electronic Model Chemistries*, version 2; 2010. <http://comp.chem.umn.edu/freqscale/version2.htm>.
- (21) Baer, T.; Hase, W. L. *Unimolecular Reaction Dynamics: Theory and Experiments*; Oxford University Press: New York, 1996.
- (22) Hase, W. L. *Acc. Chem. Res.* **1998**, *31*, 659.
- (23) Fukui, K. *J. Phys. Chem.* **1970**, *74*, 461.
- (24) Zhu, L.; Hase, W. L. *A General RRKM Program (QCPE 644), Quantum Chemistry Program Exchange*; Chemistry Department, University of Indiana: Bloomington, IN, 1993.
- (25) Ishikawa, Y.; McQuaid, M. J. *J. Mol. Struct.: THEOCHEM* **2007**, *818*, 119.
- (26) Boyle, J. M.; Uselman, B. W.; Liu, J.; Anderson, S. L. *J. Chem. Phys.* **2008**, *128*, 114304.
- (27) Fang, Y.; Liu, J. *J. Phys. Chem. A* **2009**, *113*, 11250.
- (28) Hase, W. L.; Bolton, K.; de Sainte Claire, P.; Duchovic, R. J.; Hu, X.; Komornicki, A.; Li, G.; Lim, K.; Lu, D.; Peslherbe, G. H.; Song, K.; Swamy, K. N.; Vande Linde, S. R.; Varandas, A.; Wang, H.; Wolf, R. J. *VENUS99: A General Chemical Dynamics Computer Program*; Texas Tech University: Lubbock, TX, 1999.
- (29) Bacskay, G. B. *Chem. Phys.* **1981**, *61*, 385.
- (30) Lias, S. G. Ionization Energy Evaluation. In *NIST Standard Reference Database Number 69*; Linstrom, P. J., Mallard, W. G., Eds.; National Institute of Standards and Technology: Gaithersburg, MD, 2003. <http://webbook.nist.gov>.
- (31) Laaksonen, L. *gOpenMol*, 3.0 ed.; Center for Scientific Computing: Espoo, Finland, 2005. Available at www.csc.fi/gopenmol/.
- (32) Liu, J.; Song, K.; Hase, W. L.; Anderson, S. L. *J. Phys. Chem. A* **2005**, *109*, 11376.
- (33) Liu, J.; Song, K.; Hase, W. L.; Anderson, S. L. *J. Am. Chem. Soc.* **2004**, *126*, 8602.
- (34) Liu, J.; Song, K.; Hase, W. L.; Anderson, S. L. *J. Chem. Phys.* **2003**, *119*, 3040.
- (35) Liu, J.; Uselman, B.; Boyle, J.; Anderson, S. L. *J. Chem. Phys.* **2006**, *125*, 133115.
- (36) Liu, J.; Anderson, S. L. *Phys. Chem. Chem. Phys.* **2009**, *11*, 8721.
- (37) Fang, Y.; Liu, F.; Bennett, A.; Ara, S.; Liu, J. *J. Phys. Chem. B* **2011**, *115*, 2671.
- (38) Untch, A.; Schinke, R.; Cotting, R.; Huber, J. R. *J. Chem. Phys.* **1993**, *99*, 9553.
- (39) Miller, W. H.; Hase, W. L.; Darling, C. L. *J. Chem. Phys.* **1989**, *91*, 2863.
- (40) Klapötke, T. M. Personal communication, 2010.
- (41) Herath, N.; Suits, A. G. *J. Phys. Chem. Lett.* **2010**, *2*, 642.
- (42) Seminario, J. M.; Politzer, P. *Int. J. Quantum Chem., Quantum Chem. Symp.* **1992**, *26*, 497.
- (43) Mebel, A. M.; Hsu, C.-C.; Lin, M. C.; Morokuma, K. *J. Chem. Phys.* **1995**, *103*, 5640.
- (44) Zhu, L.; Hase, W. L. *Chem. Phys. Lett.* **1990**, *175*, 117.
- (45) Meyer, F.; Khan, F. A.; Armentrout, P. B. *J. Am. Chem. Soc.* **1995**, *117*, 9740.
- (46) More, M. B.; Glendening, E. D.; Ray, D.; Feller, D.; Armentrout, P. B. *J. Phys. Chem.* **1996**, *100*, 1605.
- (47) Ray, D.; Feller, D.; More, M. B.; Glendening, E. D.; Armentrout, P. B. *J. Phys. Chem.* **1996**, *100*, 16116.
- (48) Rodgers, M. T.; Armentrout, P. B. *J. Chem. Phys.* **1998**, *109*, 1787.
- (49) Rodgers, M. T.; Ervin, K. M.; Armentrout, P. B. *J. Chem. Phys.* **1997**, *106*, 4499.
- (50) Liu, J.; Devener, B. V.; Anderson, S. L. *J. Chem. Phys.* **2002**, *117*, 8292.